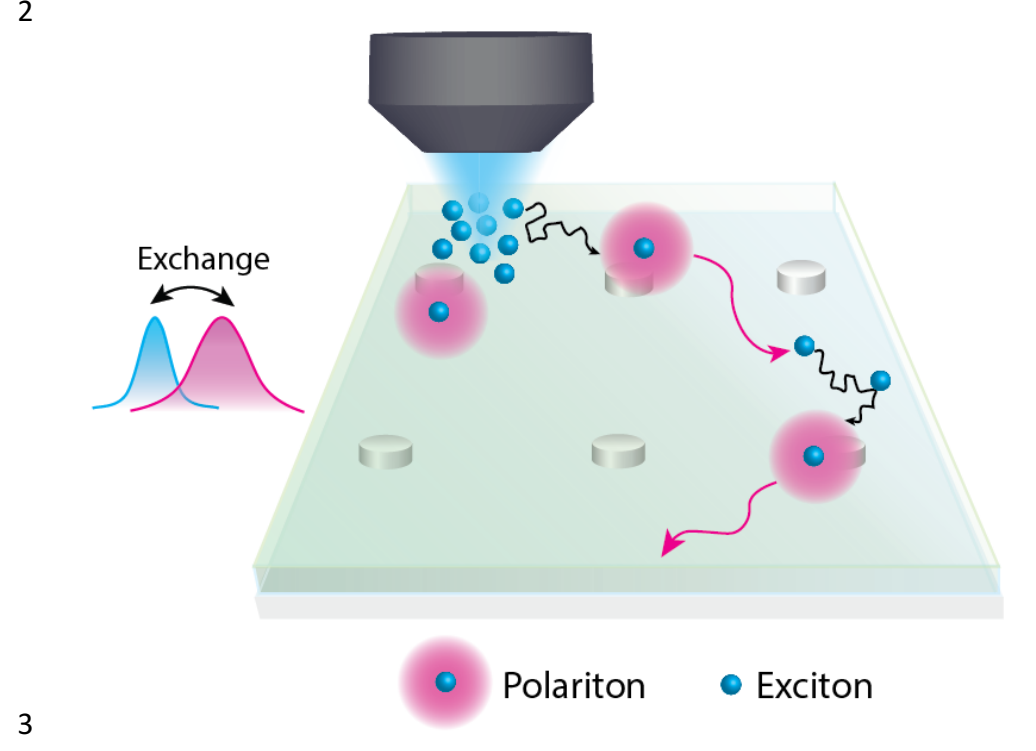
Enhanced Two-Dimensional Exciton Propagation 1 via Strong Light-Matter Coupling with Surface Lattice Plasmons 2 3 4 Linrui Jin¹, Alexander D. Sample², Dewei Sun¹, Yao Gao³, Shibin Deng¹, Ran Li⁴, Letian Dou³, Teri W. Odom^{2,4,5}, Libai Huang¹* 5 ¹ Department of Chemistry, Purdue University, West Lafayette, Indiana 47907, United States 6 7 ² Department of Chemistry, Northwestern University, Evanston, Illinois 60208, United States ³ Davidson School of Chemical Engineering, Purdue University, West Lafayette, Indiana 47907, 8 9 **United States** 10 ⁴ Department of Materials Science and Engineering, Northwestern University, Evanston, Illinois 60208, United States 11 ⁵ Graduate Program in Applied Physics, Northwestern University, Evanston, Illinois 60208, 12 **United States** 13 14 15 *Corresponding author. E-mail: libai-huang@purdue.edu

Abstract:

Exciton-polaritons—hybrid exciton-photon quasi-particles—have enabled exciting long-range coherent transport by taking advantage of the properties of their photonic component. However, most experimental demonstrations of strong coupling have been based on semiconductor Fabry-Pérot microcavities. Here we report an open and versatile exciton-polariton platform by integrating two-dimensional lead halide perovskites with plasmonic nanoparticle arrays, which support hybridization between excitons and surface lattice resonances in the strong coupling regime. Benefit from the open architecture, we directly visualized polariton-enhanced exciton transport via angle-dependent transient absorption microscopy measurements. The observed transport enhancement extends into picosecond time scale, leading to more than one order of magnitude improvement of exciton migration, from ~ 10 nm to hundreds of nanometers. We proposed a polariton-mediated exciton transport model and obtained an average polariton velocity of $\sim 1 \times 10^6$ m/s for states with $\sim 40\%$ photonic fraction. These results demonstrate plasmonic particle arrays as a versatile and adaptable cavity to enhance exciton transport.

Keywords: exciton polariton transport; strong light-matter coupling; plasmonic nanoparticle
arrays, ultrafast microscopy;

1 TOC 2



Introduction

Exciton transport governs the efficiency of optoelectronic devices such as solar cells, light-emitting diodes and excitonic transistors.¹⁻³ However, in the solid state, the effective migration of excitons is usually limited by phonon scattering, material disorder, and thermal fluctuations.⁴ By forming exciton-polaritons (hybrid exciton-photon quasi-particles), strong light-matter coupling provides a new means to overcome the limitations imposed by disorder and scattering by taking advantage of the long-range coherence of photons.⁵⁻¹¹ Thus far, research efforts have been largely focused on semiconductor microcavities, using quantum well excitons sandwiched in vertical Fabry-Pérot (FP) cavities made of thick stacks of distributed Bragg reflectors.^{12, 13} Phase transitions to quantum condensed phases such as Bose-Einstein condensation (BEC) and superfluidity have been successfully achieved in this type of structure.¹⁴⁻¹⁸ However, such microcavities are closed architectures that are challenging to efficiently probe dynamics inside the cavity. Their >100 μm scale makes them too large to be integrated in on-chip devices.

Plasmonic nanoparticle (NP) arrays uniquely combine plasmonic and photonic attributes, presenting a highly tunable two-dimensional (2D) open-cavity platform that can overcome the limitations of FP cavities to enhance exciton transport. 19-23 When arranged into 2D periodic lattices, localized surface plasmon (LSP) resonances in individual metal NPs interact with each other through LSP-induced electric fields. When the distance between NPs satisfies a Bragg condition, these collective LSP modes take on the diffractive character of the 2D photonic cavity modes supported by the lattice to form lattice plasmons (also known as surface lattice resonances, SLRs) that can be delocalized over substantial distances.^{22, 24} SLR can propagate in the plane of the array coherently at nearly the speed of light and are delocalized over substantial distances (greater than 100 µm). 24-26 Formation of exciton-polaritons has been observed when coupling plasmonic NP arrays with organic molecules, 27-30 metal-organic frameworks (MOFs), 31 quantum dots, ^{32, 33} carbon nanotubes, ^{34, 35} 2D Ruddlesden-Popper phase perovskites, ³⁶ and transition metal dichalcogenides (TMDCs).^{37, 38} Among the excitonic materials allowing room-temperature exciton-polariton operation, 2D perovskites are of great interests because of their structural versatility, ease of fabrication, and high oscillator strength that promotes strong coupling.³⁹ Moreover, the self-assembled multi-quantum well structure allows tunable thickness while maintaining stable direct excitons, which can be useful to tune the coupling strength. 12, 36, 40 2D perovskites have been employed to demonstrate polariton condensation and strong polariton interaction in FP cavities,^{41, 42} but with few report of exciton-polariton on plasmonic arrays.³⁶ Specifically, how exciton transport is modified via strong light-matter interaction is largely unknown. Because the polaritonic states have lifetimes of 100s of femtoseconds or shorter, questions remain regarding the time and length scale of the coherent transport. Theoretical calculations have suggested the scattering between the bright polaritons and the dark excitonic states play a key role in controlling the overall population dynamics.⁴³

Here we investigated the interplay between polariton and exciton transport using angle-dependent spectroscopy and microscopy. 2D organic-inorganic perovskite quantum wells were coupled to arrays of silver nanoparticles to realize exciton-polaritons at room temperature with Rabi splitting as large as 185 meV. Utilizing transient absorption microscopy with a temporal resolution of ~ 300 fs and a spatial precision of ~ 50 nm, we showed that the population exchange between the polariton and exciton states led to enhanced transport of the entire exciton population over picosecond or longer timescales. While excitation spends the majority of the time in the dark excitonic states that migrate incoherently, the nonzero probability of transition back to the polaritons states allows excitations to propagate with a much higher speed, albeit for only a brief time.

Results and Discussion

To investigate exciton-polariton transport supported by SLR, we coupled a 2D perovskite $(4\text{Tm})_2\text{SnI}_4^{44}$ (4Tm stands for 2-(3‴,4′-dimethyl-[2,2′:5′,2″:5″,2‴'-quaterthiophen]-5-yl)ethan-1-ammonium ligand) to an Ag NP array. The conjugated 4Tm ligands provide superior stability for experiments with intense laser excitation. ⁴⁴ Fig. 1a schematically illustrates the structure of the hybrid system, where the 2D perovskite of desired thickness was spin-coated directly onto the array, followed by a 300-nm layer of polymethyl methacrylate (PMMA) index matching medium (see Methods for more details). A fluorescence microscope image of the hybrid system is displayed in Fig. S1, showing the overall uniformity of the thin film. The optical response of the 2D perovskite thin film is dominated by a sharp exciton resonance at 620 nm (Fig. 1b). Due to quantum and dielectric confinement, the excitons are strongly bound and confined in the SnI₄²⁻ inorganic layer, with a binding energy estimated to be ~ 180 meV (see Supplementary Fig. S2). We fabricated Ag arrays with periodicity = 400 nm, diameter = 80 nm, height = 70 nm, and adopted PMMA index matching medium (n = 1.46) to have the SLR close to the exciton resonance. The

- 1 resulting detuning between the 2D excitons and SLR at zero momentum (k) is around -100 meV.
- 2 The array periodicity was confirmed by scanning electron microscope (SEM) and atomic force
- 3 microscope (AFM) (see supplementary Fig. S3, S4).

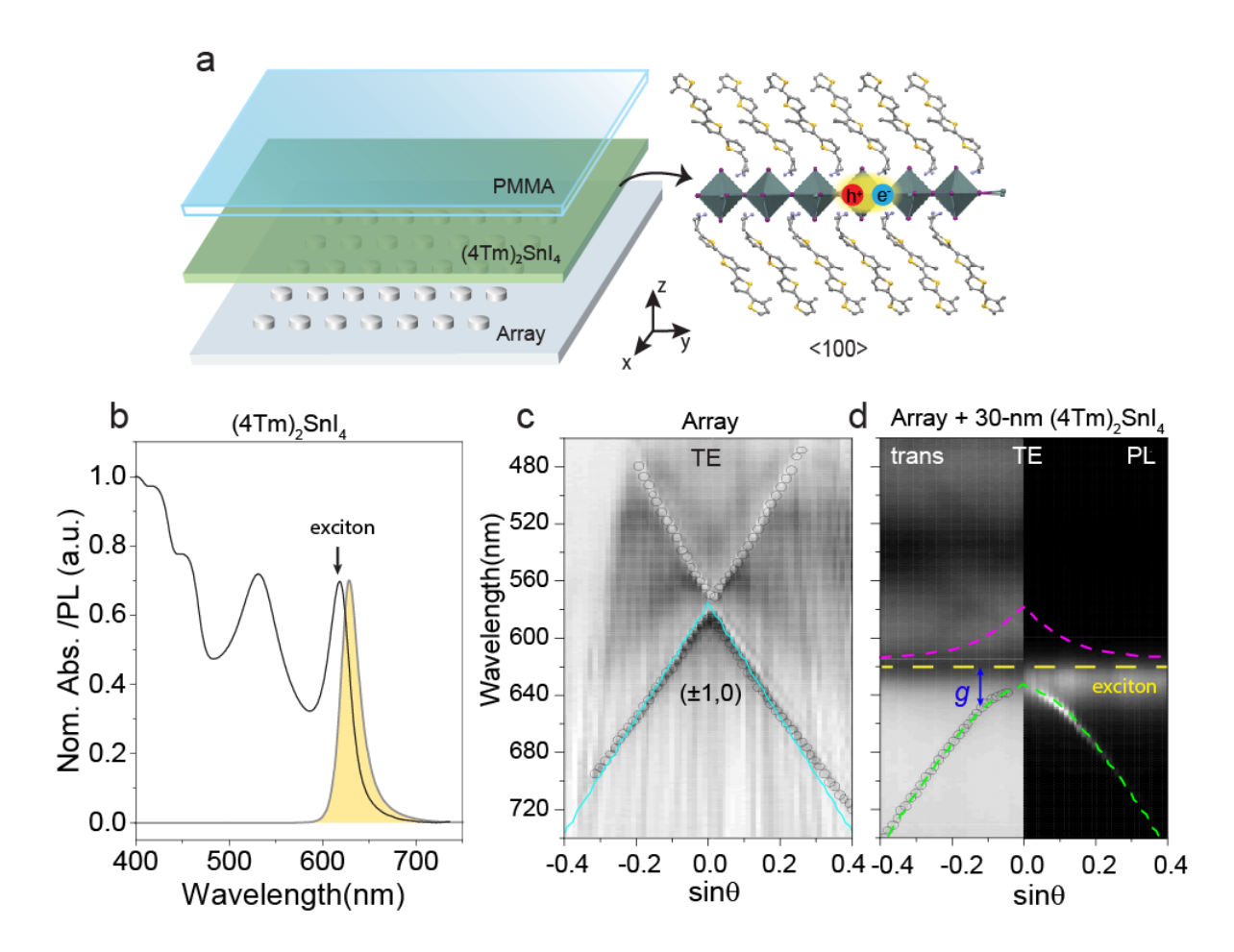


Figure 1. Exciton-polaritons formation in 2D perovskite-Ag NP array hybrid system. (a) Depiction of the sample structure, where the Ag NP array is covered with $(4\text{Tm})_2\text{SnI}_4$ film with PMMA superstrate. (b) Normalized absorption and photoluminescence spectra of a pristine $(4\text{Tm})_2\text{SnI}_4$ thin film. (c) Angle-resolved transmittance spectrum of a bare array of 400 nm periodicity with PMMA superstrate. Circles are the extracted local minima, and the cyan line indicates the theoretical SLR dispersion used in the coupled oscillator model. (d) Angle-resolved transmittance and photoluminescence (PL) spectrum of a hybrid system with 30-nm thick perovskite film. Circles mark the extracted local minima of each angle. Yellow dashed line indicates exciton resonance of $(4\text{Tm})_2\text{SnI}_4$ perovskite. Green dashed line indicates the fit to the local minima using coupled oscillator model and magenta dashed line is the simulated upper polariton dispersion. Navy arrow marks the coupling strength g at the angle of zero detuning. All dispersion measurements were performed under transverse-electric (TE) polarization.

Angle-resolved transmittance and photoluminescence (PL) spectroscopy were performed to characterize the SLR, exciton, and exciton-polariton dispersions. Fig. 1c shows the angle-

resolved transmittance spectrum of an uncoupled array with PMMA superstrate, where local minima of the transmittance follow the $(\pm 1,0)$ modes of the Rayleigh-Wood anomalies.^{45, 46} For the perovskite-only thin film, the angle-resolved measurement shows no angle dependence as expected from much heavier exciton effective mass, with the transmission minimum centered at λ = 620 nm and the PL centered at λ = 630 nm (Fig. S5). Both the bare array and perovskite-only dispersions are clearly different from that of the hybrid $(4\text{Tm})_2\text{SnI}_4$ perovskite-Ag array.

By stacking (4Tm)₂SnI₄ of different thickness on the array, the exciton-SLR interaction was tuned from weak to strong coupling regime. The perovskite thickness was controlled by varying the concentration of the spin-coated solution and was verified by AFM (Fig. S6) and absorption intensity (Fig. S7). In the hybrid structure with the 8-nm thick perovskite, no anticrossing was observed in the angle-resolved transmittances spectrum (Fig. S8a). In addition, the enhanced PL due to Purcell effect follows the dispersion of the bare array, which indicates that interaction is in the weak coupling regime. In contrast, anti-crossing between exciton resonance and (±1, 0) mode was observed in both the 20-nm thick (Fig. 1d) and 30-nm thick (Fig. S8c) samples as a result of strong light-matter interaction. The local minima of the transmittance were extracted and fitted to a coupled oscillator model to obtain coupling strength of 150 meV and 185 meV, for the 20-nm and 30-nm samples, respectively (green dashed lines in Figure 1d). Emissions from the strongly coupled sample follow the lower polariton (LP) dispersion extracted in transmittance, as shown in the angle resolved PL spectra in the right halves of Fig. 1d. No emission from upper polariton (UP) was observed due to the fast relaxation of UP.⁴⁷

Transient absorption (TA) spectroscopy was first used to characterize the dynamics of excitons and polaritons. Under a non-resonant pump at 400 nm, the optical response of pristine and strongly coupled samples are compared. Fig. 2a shows the TA spectra of the control 2D perovskite thin film, where a photo-bleach band at the exciton resonance at ~ 620 nm was observed. When coupled to the Ag NP array (Fig. 2b) two bleach bands were observed at 605 nm and 640 nm and are attributed to the UP and LP, respectively. The TA spectra of the coupled system were also different from those of the array-only sample (Fig. S9), where only SLR resonance was observe. We compared the TA spectra at 1 ps time delay of both the perovskite only film and the coupled system (Fig. 2c). The energy difference between the UP and LP is smaller than the Rabi splitting energy shown in Fig. 1, because the largest splitting occurs at $sin\theta$

 \approx 0.12 due to the non-zero detuning, and this angle is not covered by the collection range in the

2 TA measurements ($sin\theta < 0.10$).

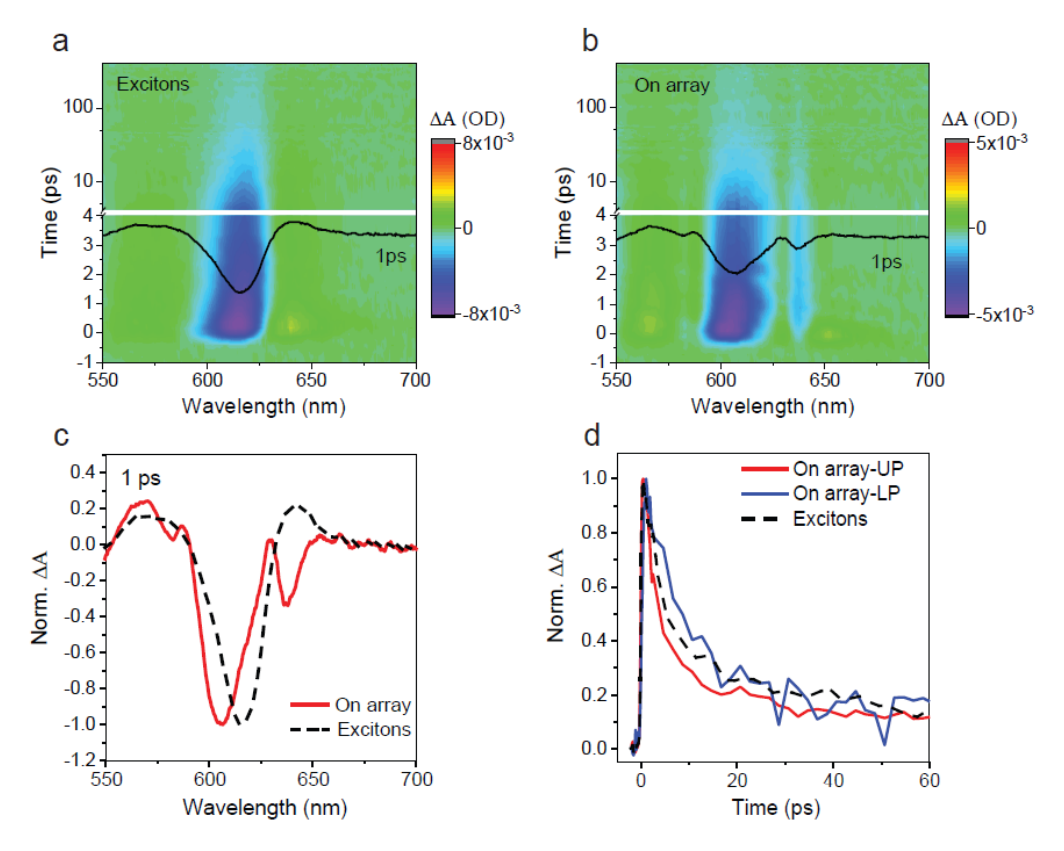


Figure 2. Transient absorption spectral feature of the strongly coupled hybrid system. (a) TA pseudocolor map of the pristine 20-nm $(4Tm)_2SnI_4$ perovskite. (b) TA pseudo-color map of the 20-nm thick $(4Tm)_2SnI_4$ on array. (c) TA spectra at 1 ps time delay extracted from (a) and (b), showing exciton bleach signal on pristine sample while two branches are observed on array. (d) TA kinetics of 605 nm and 640 nm extracted from (a), plotted with pristine exciton decay kinetics at 620 nm extracted from (b).

The TA spectra agree well with linear transmission spectrum the strongly coupled system taken over the same angle range of $sin\theta < 0.1$ as shown in Fig. S10. The larger amplitude of the UP bleach than the LP can be explained by the positive detuning between the SLR and exciton resonance, resulting in UP being more SLR-like and gain higher extinction.^{31, 36} Fig. 2d depicts the TA kinetics extracted at UP and LP resonances, plotted with exciton-only decay kinetics. TA signal at both polariton resonances persists up to tens of ps, with faster decay probed at the UP resonance due to higher photon character and possibly more scattering channels.⁴⁷ The polariton lifetime in an optical cavity is expected to be governed by the shorter of the two components, usually photon kinetics, which depends on the cavity finesse (quality factor Q) through $\tau_{Photon} \approx 2Q/\omega_{SLR}$. For the arrays used in this work, $Q \approx 100$ which corresponds to ~ 0.5 ps photon lifetime.

Therefore, the observed signal over tens of ps timescale is likely not purely from polaritons but rather the result of exciton and polariton population exchange, 43, 48-50 or modified refractive index due to photoexcitation effect. The TA dynamics at delay time > 10 ps are similar for the coupled system and the perovskite-only thin film, reflecting the population equilibrium between polariton and exciton states.

We employed transient absorption microscopy (TAM) to spatially and temporally image the exciton and polariton transport in the strongly coupled system. A schematic illustration of the TAM instrument is shown in Fig. S11. To image transport in both spatial and temporal domains, samples were excited non-resonantly at 500 nm with a diffraction-limited pump beam. The probe beam was scanned relative to the pump in space using a Galvanometer scanner. The pump induced change in probe transmission (ΔT) was plotted as a function of probe position to generate 2D TAM images. The probe wavelength was selected to be in resonance with either the excitons (620 nm) of perovskite-only film, or the photon-like UP (605 nm) of the strongly coupled system. Fig. 3a and 3b show the TAM images of exciton and polariton transport at delay times of 0 ps, 3 ps and 10 ps for the perovskite-only and the coupled system, respectively. The profile at time zero (n_0) corresponds to the convolution of Gaussian pump and probe beam centered at (x_0, y_0) given by $n_0 = A_0 \exp\left(-\frac{(x-x_0)^2}{2\sigma_{x,0}^2} - \frac{(y-y_0)^2}{2\sigma_{y,0}^2}\right)$, where $\sigma_{x,0}^2$ and $\sigma_{y,0}^2$ are the variance of the 2D Gaussian. At a later delay time t, the distribution broadens to $n_t = A_t \exp\left(-\frac{(x-x_0)^2}{2\sigma_{x,t}^2} - \frac{(y-y_0)^2}{2\sigma_{y,t}^2}\right)$ due to exciton and polariton transport. The mean square displacement (MSD) of the excitons and polaritons over time t is given by $\sigma_t^2 - \sigma_0^2$.

In the time range of 10 ps, no obvious exciton diffusion (< 10 nm) was observed in the perovskite-only thin film. This is expected considering the relatively small exciton diffusion constant ($\leq 0.1 \text{ cm}^2\text{s}^{-1}$) of n=1 2D perovskite from previous reports.⁵²⁻⁵⁴ Notably, when probing UP (605 nm) on the perovskite-array sample with same excitation density, much faster transport was observed. As shown in Fig. 3b, the fast expansion from the pumped area and transport of polaritons and excitons over μ m distances can be observed. The enhanced transport can be clearly observed when comparing the averaged horizontal cross section of the 2D images at 10 ps time delay of both pristine sample and the sample on the array (Fig. 3c). These results were repeated in a second measurement (Fig. S12).

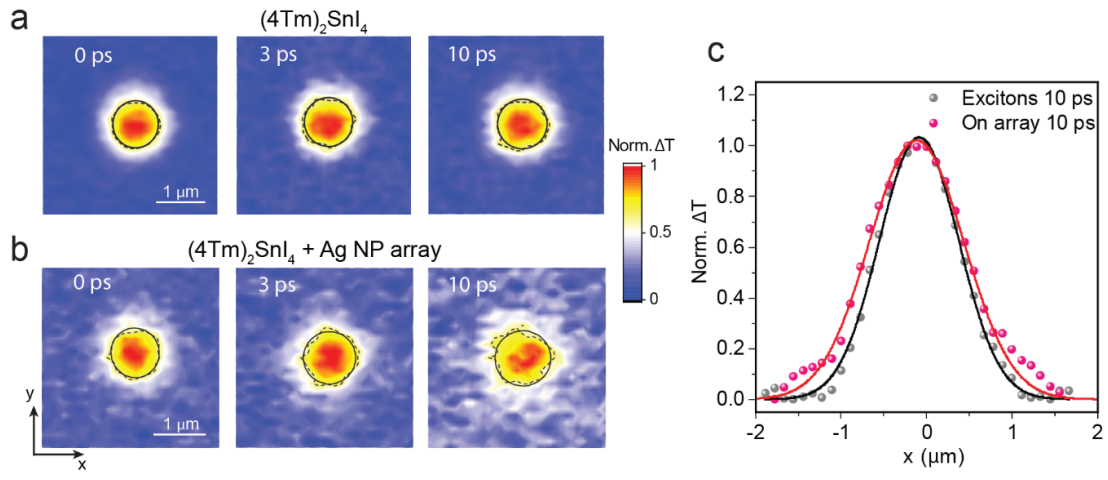


Figure 3. Transient absorption microscopy (TAM) imaging of exciton diffusion and SLR-enhanced transport. (a) The TAM images of the exciton diffusion in a pristine $(4\text{Tm})_2\text{SnI}_4$ at various delay times. (b) The TAM images of the enhanced transport in a strongly coupled hybrid system at various delay times, measured under the same condition as in (a). Pseudo color scale represents the intensity of pump-induced differential transmission (ΔT) of the probe and every image has been normalized by the peak value. The dashed lines are the radial sigma of the 2D profile, while solid lines represent the sigma of 2D Gaussian fitting result. (c) Horizontal cross section integrated along y direction from (a) and (b) at 10 ps delay time. The solid lines are fits to a Gaussian function. The profile on array (red) shows a wing that is not fully fitted to the Gaussian function, indicating a small population propagates over μ m distance. The fluence used here is 12 uJ/cm^2 .

To confirm the enhanced transport was indeed the result of exciton-polariton formation, we performed momentum-dependent TAM measurements (Fig. 4) because the photonic fraction of the polariton is expected to vary with k. We varied the collection angle by switching to an objective with smaller numerical aperture (NA) which restricted the collection angle, as illustrated in the inset of Fig. 4a. The largest momentum probe is related to θ by $k = \frac{2\pi n sin\theta}{\lambda} = \frac{2\pi NA}{\lambda}$. The TAM images collected with NA of 0.25 and 0.75 are shown in Fig. S13. Considering the isotropic nature of the $(4\text{Tm})_2\text{SnI}_4$ crystal lattice as well as the square array periodicity, the transport of exciton or polariton should be isotropic. Therefore, σ_t^2 was calculated by averaging extracted σ_{xt}^2 and σ_{yt}^2 at each delay time, and was plotted in Fig. 4a. Faster transport was observed with a collection NA of 0.25 compare to that with a collection NA of 0.75. Overall, exciton transport was observed to be enhanced significantly by coupling to the array. The MSD is increased by ~ 0.1 μ m² corresponding to an average migration distance of ~ 300 nm in 10 ps, which is more than two orders of magnitude larger than pure exciton diffusion.

The fact that transport is dependent on the collection angle suggests that polaritons play an important role. We calculated the angle-dependent photon and exciton composition of UP, namely

Hopfield coefficient $|C|^2$ and $|X|^2$, using the coupled oscillator model (details described in the Supporting Information). As shown in Fig. 4c, photon component $|C|^2$ of UP is larger at smaller collection angle. By integrating the $|C|^2$ of UP over the momentum k for the two different experimental geometries (green and yellow shaded area), we obtained that an average $|C|^2$ value of $\sim 40\%$ with a NA 0.25, which is ~ 1.2 times higher than NA of 0.75. Consistent with a larger photonic contribution and lighter effective mass, the σ_t^2 grows faster with collection NA of 0.25 (Fig. 4a). We also observed a faster decay with NA of 0.25 (Fig. 4b). A faster decay dynamics in TAM can have two origins: a shorter lifetime, and/or a quicker expansion resulting in faster decrease of population at the center.

The theoretical photon lifetime of the arrays estimated from the Q of the array is ~ 0.5 ps. The observed transport over the ps timescale is again the result of exciton and polariton population exchange (Fig. 4d). A recent theoretical work has shown significant population transfer from LP to the dark states and from exciton reservoir to UP even if the average energy difference is more than 0.3 eV.⁴³ These two process were also observed experimentally using 2D electronic spetroscopy⁴⁹ and temperature dependent measurement⁵⁰, respectively. Because the UP and LP share ground state, population in the LP also contributes to the bleach probed at the UP resonance. Thus, the transport processes imaged by TAM have contributions from exciton, UP and LP states.

To extract the parameters for polariton-enhanced exciton transport, the TAM results were simulated using a population exchange model described by the coupled rate equations below:

$$\frac{\partial n_P(x,t)}{\partial t} = D_P \nabla^2 n_P(x,t) - k_P n_P(x,t) - k_{P-e} n_P(x,t) + k_{e-P} n_e(x,t), \tag{1}$$

21
$$\frac{\partial n_e(x,t)}{\partial t} = D_e \nabla^2 n_e(x,t) + k_{P-e} n_P(x,t) - (k_{e-P} + k_e) n_e(x,t) - 2 * k_{annih} n_e^2(x,t)$$
 (2)

 D_P and D_e are the diffusion constant of polaritons and excitons, respectively. k_{P-e} and k_{e-P} are the population exchange rate between exciton and polariton states. k_P is the polariton decay rate that includes the decay through photonic leakage as well as scattering into the exciton state. We approximated k_P to be 2×10^3 ns⁻¹ using photon lifetime of the array. k_e and k_{annih} are the exciton decay rate and annihilation rate of $(4\text{Tm})_2\text{SnI}_4$, respectively. We first extracted k_e and k_{annih} by fitting the excitation density dependent TA kinetics of the perovskite-only thin film (see supplementary Fig. S14). D_e was kept at 0.1 cm²s⁻¹. During the numerical fitting process, D_e , k_e , k_{annih} and k_P were fixed while D_P , k_{P-e} and k_{e-P} were varied iteratively until the simulated exciton transport best describes all the datasets. The fitting results are plotted as solid lines in Fig.

4a and Fig. 4b along with experimental data. The parameters used in the simulation are summarized in Table S1. The extracted polariton to exciton transfer rate k_{P-e} corresponds to \sim 100 fs, on the same time scale as the cavity dephasing time and is consistent to that measured in a J-aggregate microcavity system using 2D spectroscopy⁵⁵. This picture of cooperative exciton and polariton transport picture is consistent with a recent time-domain investigation of polariton propagation in FP cavities that indicated the importance of dark states.⁹

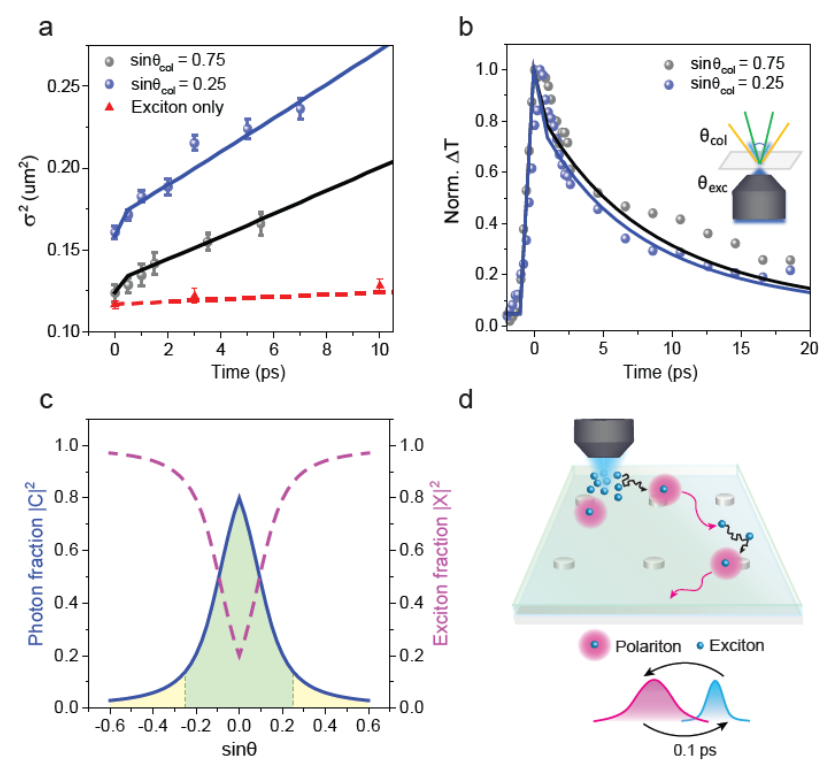


Figure 4. Angle-dependent TAM of SLR-enhanced exciton transport and the population exchange model. (a) σ_t^2 extracted from the TAM images on a strongly coupled perovskite-Ag array system measured with different collection angle (blue and grey), plotted with σ_t^2 extracted from Fig. 3a of exciton-only transport in $(4\text{Tm})_2\text{SnI}_4$ (red). Solid lines are the fits to the data using the population exchange model described in the main text. (b) Normalized transient absorption kinetics measured with different collection angle when the pump and probe beams overlap. Solid lines are the simulation results using the population exchange model. Inset: schematic illustration of the angle-dependent imaging with collection NA of 0.25 and 0.75. (c) Hopfield coefficients dispersion for the UP state in a 30-nm perovskite-Ag array system. $|X_{UP}|^2$ and $|C_{UP}|^2$ are the exciton fraction and photon fraction, respectively. Green shaded area represents the angle range with $sin\theta_{col} = 0.25$. (d) Schematic illustration of the population exchange model that lead to enhanced exciton transport. Blue spheres represent the exciton species and magenta-shaded spheres represent polariton states.

The extracted value of D_P is as large as $1600 \text{ cm}^2\text{s}^{-1}$ for the range of k accessible with a NA of 0.25, and this is equivalent to an average propagation velocity v_P of 1.4×10^6 m/s using the approximation $L_P = \sqrt{D_P \tau_P} = v_P \times \tau_P$, where L_P is the polariton propagation length and τ_P is the total loss time including radiative decay and scattering⁵. For k range with a NA of 0.75, the D_P of $1000 \text{ cm}^2\text{s}^{-1}$ corresponds to a v_P of 1.1×10^6 m/s. As a comparison, the polariton group velocity calculated from the dispersion derivate $(\frac{1}{h} \frac{dE_R}{dk})$ is $\sim 1 \times 10^8$ m/s (Fig. S15). The orders of magnitude lower effective velocity likely result from inhomogeneities due to spatially varying coupling strength: the excitons located near the nanoparticles are coupled stronger to the photons than the molecules that are away from the nanoparticles (Fig. 4d). Such inhomogeneities lead to uncertainty of in-plane wavevector $k_{||}$ and coherently propagating polaritons only occur in a certain range $k_{||}$ (where the uncertainty $\delta k_{||} < k_{||})^{56}$. The reduced effective velocities have also been reported in molecular polariton systems where inhomogeneities (such as molecular orientation) are significant; for example, in a molecule-DBR system $(0.1-0.65 \times 10^6 \text{ m/s})^9$ and in a J-aggregate microcavity $(0.2-0.4 \times 10^6 \text{ m/s})^8$ using similar TAM techniques.

Finally, the model described by Equations (1) and (2) assumes the motion is mostly diffusive and the population distribution can be described by a Gaussian function. However, population distribution of the coupled system is not purely Gaussian but rather with a small tail (about 5%) that propagates over μm distance as shown in Fig. 3b-c. The non-Gaussian behavior can be explained by heterogeneous two-state transport⁵⁷ as the purely ballistic and mostly incoherent states are expected to have different transport properties. We attributed the small tail extended over μm to the subset of polaritons within a small $k_{||}$ that propagate ballistically and thus with a higher velocity, which is consistent with previous reported μm coherence supported by SLRs⁵⁸. In two recent reports, ballistic transport was observed when photonic component is 0.5 or greater, and transit to diffusive transport when polariton is more exciton-like. ^{10, 11} In our experiments, photonic component is 0.4 or smaller and the motion observed is mostly diffusive, which is consistent with these previous reports.

Conclusion

In summary, we demonstrated Ag NP arrays act as an open cavity to enhance exciton transport. By employing angle-resolved transient absorption microscopy, we revealed that exciton

- 1 migration can be improved from ~ 10 nm to 100s of nm and even μ m in the picosecond timescale
- 2 by leveraging strong light-matter coupling with SLRs. Our results highlight the importance of
- 3 understanding interactions between excitons and polaritons, which leads to new avenues to
- 4 modulate transport properties of excitons. We employed 2D perovskites as a prototypical exciton
- 5 system; however, these results should be applicable to other excitonic materials. Unlike the
- 6 conventional FP cavities, these SLR arrays are highly flexible and configurable, which makes them
- 7 attractive for designing exciton transport for optoelectronic applications.

8 Methods

9 Fabrication of the Ag nanoparticle array

- 10 Arrays of Ag NPs were fabricated on quartz substrates using the previously reported SANE
- 11 (solvent assisted nanoscale embossing)⁵⁹ and PEEL (photolithography, etching, electron-beam
- deposition, and lift-off)⁶⁰ methods. Ag NPs were passivated with a thin layer of alumina grown
- 13 with CVD.

14 Fabrication of the (4Tm)₂SnI₄ perovskite thin films

- The synthesis of 2-(3"',4'-dimethyl-[2,2':5',2":5",2"'-quaterthiophen]-5-yl)ethan-1-ammonium
- iodide (4TmI) follows a previous published procedure⁴⁴. As synthesized 4TmI (53.0 mg, 100
- 17 μmol) and SnI₂ (23.0 mg, 50 μmol) were dissolved in 1 mL of anhydrous DMF/DMSO (10/1) at
- 18 70 °C. The (4Tm)₂SnI₄ stock solution was allowed to cool to room temperature for spin coating.
- 19 To obtain different perovskite thickness, above stock solution was diluted with DMF to be 20%,
- 20 50% and 75% concentrated. The arrays or fused silica substrates were treated with UV-ozone for
- 21 10 min before loaded into the glove box for spin coating. (4Tm)₂SnI₄ thin films were prepared by
- spin coating the solutions at 4000 rpm for 60 s, followed by thermal annealing at 180 °C on a hot
- plate for 10 min. To protect the sample as well as provide an index matching environment, PMMA
- 24 (MicroChem) was finally spin coated onto the sample at 1500 r.p.m. for 45 s.

25 Angle-resolved transmittance and photoluminescence (PL) measurements

- The angle-resolved transmittance or PL was measured with a home-built setup based on Fourier
- optics. Briefly, a stabilized tungsten-halogen lamp (Thorlabs) was used as white light source and
- 28 is focus onto the sample using a $40 \times$ objective (Nikon, NA = 0.60), then the transmitted light is
- collected by another objective (Olympus, $50\times$, NA = 0.95). The back focal plane of the collection
- 30 objective was transformed into an intermediate image plane by a tube lens, followed by a Fourier
- 31 lens to directly project the Fourier image onto a charge-coupled device (CCD, Andor Newton 920)

- 1 detector after the spectrometer (Andor Shamrock 303i). The same spectrometer and CCD
- 2 combination were used for angle-resolved PL measurement. A picosecond pulse laser of 447 nm
- 3 wavelength was used as the excitation light. The same 50× objective was employed to focus the
- 4 excitation beam on the sample and to collect the back-scattered PL light, which was similarly
- 5 projected on the CCD with spectral and angular resolution. A linear polarizer was positioned in
- 6 front of the entrance slit of the spectrometer to selectively measure the transverse-electric (TE) or
- 7 transverse-magnetic (TM) mode.

8 Transient absorption spectroscopy (TA)

- 9 TA spectra of the perovskite only, bare array and perovskite-array samples were measured by a
- home-built femtosecond pump-probe system. The fundamental 1030 nm laser pulses (250 fs pulse
- duration) were generated by a 750 kHz amplified Yb:KGW laser system (PHAROS, Light
- 12 Conversion Ltd.). To generate a broad-band probe beam, a fraction of the 1030 nm fundamental
- output was focused on a YAG crystal, which covered the spectral range of 450–800 nm. The
- 14 remaining fundamental laser was directed towards an optical parametric amplifier (OPA,
- ORPHEUS-Twins, Light Conversion Ltd.) to create wavelength-tunable pump pulses with an
- approximate bandwidth of 10 nm. This was then modulated by an optical chopper (MC200B,
- 17 Thorlabs) with a frequency of 195 Hz. In order to delay the probe beam relative to the pump beam,
- a linear stepper motor stage (Newport) was used. Both the pump and probe beams were focused
- on the sample using a $5 \times$ objective (NA = 0.1, Olympus). The change in transmission of the probe
- signal ($\Delta T/T$) was collected by a 20× objective (NA = 0.45, Olympus) and detected using an array
- 21 detector (Exemplar LS, B&W Tek).

22 Transient absorption microscopy (TAM)

- The details of the home-built TAM setup (Fig. S10) were described in a previous publication⁶¹.
- 24 Briefly, two independent optical parametric amplifiers (OPAs) with a frequency of 750 kHz and
- pulse durations of 200-300 fs (Light Conversion) were utilized to generate pump and probe beams.
- The spatial filters were employed to optimize the Gaussian profile of the beams. The pump beam
- was modulated at 100 kHz using an acousto-optic modulator (Gooch and Housego, R23080-1).
- 28 The relative delay between the pump and probe pulses was controlled by a mechanical translation
- stage (Thorlabs, DDS600-E). To produce diffusion images, the probe beam was scanned in the x
- and y directions near the pump beam with a pair of Galvo mirrors (Thorlabs GVS012). A 40×
- objective (NA = 0.60, Nikon) was used to focus both the pump and probe beams on the sample.

- 1 The transmitted probe light was collected either by an objective (NA = 0.25, Nikon) or a condenser
- 2 (NA = 0.75, Thorlabs), and the detector was an avalanche photodiode (APD) (Hamamatsu, C5331-
- 3 04). The pump-induced change in probe transmission (ΔT) was extracted by a lock-in amplifier
- 4 (SR830, SRS Inc.).

6 The authors declare no competing financial interests.

7

8

Supporting Information

- 9 Additional experimental details and methods including fluorescence microscope image, low-
- 10 temperature reflectance spectrum, atomic force microscope and scanning electron microscope
- 11 results, additional angle-resolved characterization, determination of sample thickness, additional
- 12 transient absorption spectra and microscope results, illustration of experimental setup, and
- coupled-oscillator model details.

14

15

Acknowledgement

- We thank Enzheng Shi for valuable discussions and initial trials of the idea. We acknowledge the
- support from Purdue Life Science Microscopy Facility and Research Instrumentation Center.

18

- 19 **Funding Sources** L.J. and L.H. acknowledge the funding from the National Science Foundation,
- through award NSF-CHE 2154388. A.D.S. and T.W.O. were funded by the Office of Naval
- 21 Research (ONR N00014-21-1-2289) and made use of the NUFAB and EPIC facilities of
- 22 Northwestern University's NUANCE Center, which have received support from the SHyNE
- 23 Resource (NSF ECCS-2025633), the IIN, and Northwestern's MRSEC Program (NSF DMR-
- 24 1720139). Y.G. and L.D. acknowledge the support from US Office of Naval Research under award
- 25 N00014-19-1-2296.

26 References

- 27 1. Gregg, B. A., Excitonic solar cells. ACS Publications: 2003; Vol. 107, pp 4688-4698.
- 28 2. Akselrod, G. M.; Deotare, P. B.; Thompson, N. J.; Lee, J.; Tisdale, W. A.; Baldo, M. A.;
- 29 Menon, V. M.; Bulović, V., Visualization of exciton transport in ordered and disordered
- 30 molecular solids. *Nat. Commun.* **2014,** *5* (1), 3646.
- 31 3. High, A. A.; Novitskaya, E. E.; Butov, L. V.; Hanson, M.; Gossard, A. C., Control of exciton
- fluxes in an excitonic integrated circuit. Science 2008, 321 (5886), 229-231.

- 4. Nag, B., *Electron Transport In Compound Semiconductors*. Springer Berlin, Heidelberg,
- 2 1980; Vol. 11, p XVI, 464.
- 5. Myers, D. M.; Mukherjee, S.; Beaumariage, J.; Snoke, D. W.; Steger, M.; Pfeiffer, L. N.;
- 4 West, K., Polariton-enhanced exciton transport. *Phys. Rev. B* **2018**, *98* (23).
- 5 6. Hou, S.; Khatoniar, M.; Ding, K.; Qu, Y.; Napolov, A.; Menon, V. M.; Forrest, S. R.,
- 6 Ultralong-Range Energy Transport in a Disordered Organic Semiconductor at Room
- 7 Temperature Via Coherent Exciton-Polariton Propagation. Adv. Mater. 2020, 32 (28), e2002127.
- 8 7. Lerario, G.; Ballarini, D.; Fieramosca, A.; Cannavale, A.; Genco, A.; Mangione, F.; Gambino,
- 9 S.; Dominici, L.; De Giorgi, M.; Gigli, G.; Sanvitto, D., High-speed flow of interacting organic
- 10 polaritons. *Light Sci. Appl.* **2017**, *6* (2), e16212.
- 8. Rozenman, G. G.; Akulov, K.; Golombek, A.; Schwartz, T., Long-Range Transport of Organic
- Exciton-Polaritons Revealed by Ultrafast Microscopy. *ACS Photonics* **2017**, *5* (1), 105-110.
- 9. Pandya, R.; Ashoka, A.; Georgiou, K.; Sung, J.; Jayaprakash, R.; Renken, S.; Gai, L.; Shen,
- 14 Z.; Rao, A.; Musser, A. J., Tuning the Coherent Propagation of Organic Exciton-Polaritons
- through Dark State Delocalization. Adv. Sci. 2022, 9 (18), 2105569.
- 16 10. Balasubrahmaniyam, M.; Simkhovich, A.; Golombek, A.; Sandik, G.; Ankonina, G.;
- 17 Schwartz, T., From enhanced diffusion to ultrafast ballistic motion of hybrid light–matter
- 18 excitations. *Nat. Mater.* **2023**, *22* (3), 338-344.
- 19 11. Xu, D.; Mandal, A.; Baxter, J. M.; Cheng, S.-W.; Lee, I.; Su, H.; Liu, S.; Reichman, D. R.;
- Delor, M., Ultrafast imaging of coherent polariton propagation and interactions. 2022,
- 21 *arXiv.2205.01176* arXiv preprint https://arxiv.org/abs/2205.01176 (accessed 04/17/2023).
- 22 12. Deng, H.; Haug, H.; Yamamoto, Y., Exciton-polariton Bose-Einstein condensation. Rev.
- 23 *Mod. Phys.* **2010,** *82* (2), 1489-1537.
- 24 13. Gibbs, H. M.; Khitrova, G.; Koch, S. W., Exciton–polariton light–semiconductor coupling
- 25 effects. *Nat. Photonics* **2011**, *5* (5), 273-273.
- 26 14. Snoke, D., Spontaneous Bose coherence of excitons and polaritons. *Science* **2002**, *298*
- **27** (5597), 1368-72.
- 28 15. Deng, H.; Weihs, G.; Santori, C.; Bloch, J.; Yamamoto, Y., Condensation of semiconductor
- 29 microcavity exciton polaritons. *Science* **2002**, *298* (5591), 199-202.
- 30 16. Kasprzak, J.; Richard, M.; Kundermann, S.; Baas, A.; Jeambrun, P.; Keeling, J. M.;
- 31 Marchetti, F. M.; Szymańska, M. H.; André, R.; Staehli, J. L.; Savona, V.; Littlewood, P. B.;
- 32 Deveaud, B.; Dang le, S., Bose-Einstein condensation of exciton polaritons. *Nature* **2006**, *443*
- 33 (7110), 409-14.
- 34 17. Balili, R.; Hartwell, V.; Snoke, D.; Pfeiffer, L.; West, K., Bose-Einstein condensation of
- 35 microcavity polaritons in a trap. *Science* **2007**, *316* (5827), 1007-10.
- 18. Amo, A.; Lefrère, J.; Pigeon, S.; Adrados, C.; Ciuti, C.; Carusotto, I.; Houdré, R.; Giacobino,
- E.; Bramati, A., Superfluidity of polaritons in semiconductor microcavities. *Nat. Phys.* **2009**, *5*
- 38 (11), 805-810.
- 39 19. Baranov, D. G.; Wersäll, M.; Cuadra, J.; Antosiewicz, T. J.; Shegai, T., Novel
- 40 Nanostructures and Materials for Strong Light–Matter Interactions. ACS Photonics 2017, 5 (1),
- 41 24-42.
- 42 20. Yang, A.; Wang, D.; Wang, W.; Odom, T. W., Coherent Light Sources at the Nanoscale.
- 43 Annu. Rev. Phys. Chem. **2017**, 68 (1), 83-99.
- 44 21. Wang, W.; Ramezani, M.; Väkeväinen, A. I.; Törmä, P.; Rivas, J. G.; Odom, T. W., The rich
- 45 photonic world of plasmonic nanoparticle arrays. *Mater. Today* **2018**, *21* (3), 303-314.

- 1 22. Hakala, T. K.; Moilanen, A. J.; Väkeväinen, A. I.; Guo, R.; Martikainen, J.-P.; Daskalakis, K.
- 2 S.; Rekola, H. T.; Julku, A.; Törmä, P., Bose–Einstein condensation in a plasmonic lattice. *Nat.*
- 3 *Phys.* **2018,** *14* (7), 739-744.
- 4 23. Kravets, V. G.; Kabashin, A. V.; Barnes, W. L.; Grigorenko, A. N., Plasmonic Surface
- 5 Lattice Resonances: A Review of Properties and Applications. Chem. Rev. 2018, 118 (12), 5912-
- 6 5951.
- 7 24. Zou, S.; Schatz, G. C., Metal nanoparticle array waveguides: Proposed structures for
- 8 subwavelength devices. *Phys. Rev. B* **2006**, *74* (12), 125111.
- 9 25. Rekola, H. T.; Hakala, T. K.; Törmä, P., One-Dimensional Plasmonic Nanoparticle Chain
- 10 Lasers. ACS Photonics **2018**, 5 (5), 1822-1826.
- 26. Cherqui, C.; Bourgeois, M. R.; Wang, D.; Schatz, G. C., Plasmonic Surface Lattice
- 12 Resonances: Theory and Computation. *Acc. Chem. Res.* **2019**, *52* (9), 2548-2558.
- 27. Väkeväinen, A. I.; Moerland, R. J.; Rekola, H. T.; Eskelinen, A. P.; Martikainen, J. P.; Kim,
- D. H.; Törmä, P., Plasmonic Surface Lattice Resonances at the Strong Coupling Regime. *Nano*
- 15 *Lett.* **2014,** *14* (4), 1721-1727.
- 28. Shi, L.; Hakala, T. K.; Rekola, H. T.; Martikainen, J. P.; Moerland, R. J.; Törmä, P., Spatial
- 17 Coherence Properties of Organic Molecules Coupled to Plasmonic Surface Lattice Resonances in
- the Weak and Strong Coupling Regimes. *Phys. Rev. Lett.* **2014**, *112* (15), 153002.
- 19 29. Rodriguez, S. R. K.; Rivas, J. G., Surface lattice resonances strongly coupled to Rhodamine
- 20 6G excitons: tuning the plasmon-exciton-polariton mass and composition. Opt. Express 2013, 21
- 21 (22), 27411-27421.
- 30. Berghuis, A. M.; Tichauer, R. H.; de Jong, L. M. A.; Sokolovskii, I.; Bai, P.; Ramezani, M.;
- 23 Murai, S.; Groenhof, G.; Gomez Rivas, J., Controlling Exciton Propagation in Organic Crystals
- through Strong Coupling to Plasmonic Nanoparticle Arrays. ACS Photonics 2022, 9 (7), 2263-
- 25 2272.
- 26 31. Sample, A. D.; Guan, J.; Hu, J.; Reese, T.; Cherqui, C. R.; Park, J.-E.; Freire-Fernández, F.;
- Schaller, R. D.; Schatz, G. C.; Odom, T. W., Strong Coupling Between Plasmons and Molecular
- 28 Excitons in Metal–Organic Frameworks. *Nano Lett.* **2021,** *21* (18), 7775-7780.
- 29 32. Yadav, R. K.; Bourgeois, M. R.; Cherqui, C.; Juarez, X. G.; Wang, W.; Odom, T. W.;
- 30 Schatz, G. C.; Basu, J. K., Room Temperature Weak-to-Strong Coupling and the Emergence of
- 31 Collective Emission from Quantum Dots Coupled to Plasmonic Arrays. ACS Nano 2020, 14 (6),
- 32 7347-7357.
- 33. Yadav, R. K.; Otten, M.; Wang, W.; Cortes, C. L.; Gosztola, D. J.; Wiederrecht, G. P.; Gray,
- 34 S. K.; Odom, T. W.; Basu, J. K., Strongly Coupled Exciton-Surface Lattice Resonances Engineer
- 35 Long-Range Energy Propagation. *Nano Lett.* **2020,** *20* (7), 5043-5049.
- 34. Zakharko, Y.; Graf, A.; Zaumseil, J., Plasmonic Crystals for Strong Light-Matter Coupling in
- 37 Carbon Nanotubes. *Nano Lett.* **2016**, *16* (10), 6504-6510.
- 35. Zakharko, Y.; Rother, M.; Graf, A.; Hahnlein, B.; Brohmann, M.; Pezoldt, J.; Zaumseil, J.,
- 39 Radiative Pumping and Propagation of Plexcitons in Diffractive Plasmonic Crystals. *Nano Lett*.
- **2018,** *18* (8), 4927-4933.
- 41 36. Park, J. E.; Lopez-Arteaga, R.; Sample, A. D.; Cherqui, C. R.; Spanopoulos, I.; Guan, J.;
- 42 Kanatzidis, M. G.; Schatz, G. C.; Weiss, E. A.; Odom, T. W., Polariton Dynamics in Two-
- Dimensional Ruddlesden-Popper Perovskites Strongly Coupled with Plasmonic Lattices. ACS
- 44 Nano **2022**, 16 (3), 3917-3925.

- 1 37. Liu, W.; Lee, B.; Naylor, C. H.; Ee, H. S.; Park, J.; Johnson, A. T.; Agarwal, R., Strong
- 2 Exciton-Plasmon Coupling in MoS2 Coupled with Plasmonic Lattice. *Nano Lett.* **2016,** *16* (2),
- 3 1262-9.
- 4 38. Liu, W.; Wang, Y.; Zheng, B.; Hwang, M.; Ji, Z.; Liu, G.; Li, Z.; Sorger, V. J.; Pan, A.;
- 5 Agarwal, R., Observation and Active Control of a Collective Polariton Mode and Polaritonic
- 6 Band Gap in Few-Layer WS2 Strongly Coupled with Plasmonic Lattices. *Nano Lett.* **2020,** *20*
- 7 (1), 790-798.
- 8 39. Su, R.; Fieramosca, A.; Zhang, Q.; Nguyen, H. S.; Deleporte, E.; Chen, Z.; Sanvitto, D.;
- 9 Liew, T. C. H.; Xiong, Q., Perovskite semiconductors for room-temperature exciton-polaritonics.
- 10 *Nat. Mater.* **2021,** *20* (10), 1315-1324.
- 40. Ribeiro, R. F.; Martinez-Martinez, L. A.; Du, M.; Campos-Gonzalez-Angulo, J.; Yuen-Zhou,
- 12 J., Polariton chemistry: controlling molecular dynamics with optical cavities. *Chem. Sci.* **2018**, 9
- 13 (30), 6325-6339.
- 41. Fieramosca, A.; Polimeno, L.; Ardizzone, V.; De Marco, L.; Pugliese, M.; Maiorano, V.; De
- 15 Giorgi, M.; Dominici, L.; Gigli, G.; Gerace, D., Two-dimensional hybrid perovskites sustaining
- strong polariton interactions at room temperature. Sci. Adv. 2019, 5 (5), eaay 9967.
- 42. Polimeno, L.; Fieramosca, A.; Lerario, G.; Cinquino, M.; De Giorgi, M.; Ballarini, D.;
- Todisco, F.; Dominici, L.; Ardizzone, V.; Pugliese, M.; Prontera, C. T.; Maiorano, V.; Gigli, G.;
- 19 De Marco, L.; Sanvitto, D., Observation of Two Thresholds Leading to Polariton Condensation
- 20 in 2D Hybrid Perovskites. *Adv. Opt. Mater.* **2020,** 8 (16), 2000176.
- 43. Groenhof, G.; Climent, C.; Feist, J.; Morozov, D.; Toppari, J. J., Tracking Polariton
- Relaxation with Multiscale Molecular Dynamics Simulations. J. Phys. Chem. Lett. 2019, 10 (18),
- 23 5476-5483.
- 24 44. Gao, Y.; Wei, Z.; Yoo, P.; Shi, E.; Zeller, M.; Zhu, C.; Liao, P.; Dou, L., Highly Stable Lead-
- Free Perovskite Field-Effect Transistors Incorporating Linear pi-Conjugated Organic Ligands. J.
- 26 Am. Chem. Soc. **2019**, 141 (39), 15577-15585.
- 45. Wood, R. W., XLII. On a remarkable case of uneven distribution of light in a diffraction
- 28 grating spectrum. The London, Edinburgh, and Dublin Philosophical Magazine and Journal of
- 29 *Science* **1902**, *4* (21), 396-402.
- 46. Guo, R.; Hakala, T. K.; Törmä, P., Geometry dependence of surface lattice resonances in
- 31 plasmonic nanoparticle arrays. *Phys. Rev. B* **2017,** *95* (15), 155423.
- 47. Wang, H.; Wang, H. Y.; Sun, H. B.; Cerea, A.; Toma, A.; Angelis, F.; Jin, X.; Razzari, L.;
- Cojoc, D.; Catone, D.; Huang, F.; Proietti Zaccaria, R., Dynamics of Strongly Coupled Hybrid
- 34 States by Transient Absorption Spectroscopy. Adv. Funct. Mater. 2018, 28 (48).
- 48. Virgili, T.; Coles, D.; Adawi, A. M.; Clark, C.; Michetti, P.; Rajendran, S. K.; Brida, D.;
- Polli, D.; Cerullo, G.; Lidzey, D. G., Ultrafast polariton relaxation dynamics in an organic
- 37 semiconductor microcavity. *Phys. Rev. B* **2011**, *83* (24), 245309.
- 49. Takahashi, S.; Watanabe, K., Decoupling from a Thermal Bath via Molecular Polariton
- 39 Formation. J. Phys. Chem. Lett. **2020**, 11 (4), 1349-1356.
- 40 50. Coles, D. M.; Michetti, P.; Clark, C.; Adawi, A. M.; Lidzey, D. G., Temperature dependence
- of the upper-branch polariton population in an organic semiconductor microcavity. *Phys. Rev. B*
- **2011,** *84* (20), 205214.
- 43 51. Renken, S.; Pandya, R.; Georgiou, K.; Jayaprakash, R.; Gai, L.; Shen, Z.; Lidzey, D. G.; Rao,
- 44 A.; Musser, A. J., Untargeted effects in organic exciton-polariton transient spectroscopy: A
- 45 cautionary tale. *J. Chem. Phys.* **2021**, *155* (15), 154701.

- 52. Deng, S.; Shi, E.; Yuan, L.; Jin, L.; Dou, L.; Huang, L., Long-range exciton transport and
- 2 slow annihilation in two-dimensional hybrid perovskites. *Nat. Commun.* **2020,** *11* (1), 664.
- 3 53. Xiao, X.; Wu, M.; Ni, Z.; Xu, S.; Chen, S.; Hu, J.; Rudd, P. N.; You, W.; Huang, J., Ultrafast
- 4 Exciton Transport with a Long Diffusion Length in Layered Perovskites with Organic Cation
- 5 Functionalization. *Adv. Mater.* **2020,** *32* (46), e2004080.
- 6 54. Seitz, M.; Magdaleno, A. J.; Alcázar-Cano, N.; Meléndez, M.; Lubbers, T. J.; Walraven, S.
- 7 W.; Pakdel, S.; Prada, E.; Delgado-Buscalioni, R.; Prins, F., Exciton diffusion in two-
- 8 dimensional metal-halide perovskites. *Nat. Commun.* **2020,** *11* (1), 2035.
- 9 55. Mewes, L.; Wang, M.; Ingle, R. A.; Börjesson, K.; Chergui, M., Energy relaxation pathways
- between light-matter states revealed by coherent two-dimensional spectroscopy. *Commun. Phys.*
- **2020,** *3* (1).
- 12 56. Agranovich, V. M.; Litinskaia, M.; Lidzey, D. G., Cavity polaritons in microcavities
- containing disordered organic semiconductors. *Phys. Rev. B* **2003**, *67* (8), 085311.
- 57. Cao, J., Single molecule tracking of heterogeneous diffusion. *Phys. Rev. E* **2001**, *63* (4),
- 15 041101.

- 16 58. De Giorgi, M.; Ramezani, M.; Todisco, F.; Halpin, A.; Caputo, D.; Fieramosca, A.; Gomez-
- 17 Rivas, J.; Sanvitto, D., Interaction and Coherence of a Plasmon–Exciton Polariton Condensate.
- 18 *ACS Photonics* **2018**, *5* (9), 3666-3672.
- 19 59. Lee, M. H.; Huntington, M. D.; Zhou, W.; Yang, J.-C.; Odom, T. W., Programmable Soft
- Lithography: Solvent-Assisted Nanoscale Embossing. *Nano Lett.* **2011**, *11* (2), 311-315.
- 21 60. Henzie, J.; Lee, M. H.; Odom, T. W., Multiscale patterning of plasmonic metamaterials. *Nat.*
- 22 *Nanotechnol.* **2007**, *2* (9), 549-554.
- 23 61. Wang, T.; Fu, Y.; Jin, L.; Deng, S.; Pan, D.; Dong, L.; Jin, S.; Huang, L.,
- 24 Phenethylammonium Functionalization Enhances Near-Surface Carrier Diffusion in Hybrid
- 25 Perovskites. J. Am. Chem. Soc. **2020**, 142 (38), 16254-16264.